Int J Earth Sci (Geol Rundsch)
DOI 10.1007/s00531-009-0445-1

REVIEW ARTICLE

Andalusite and Na- and Li-rich cordierite in the La Costa pluton, Sierras Pampeanas, Argentina: textural and chemical evidence for a magmatic origin

Pablo H. Alasino · Juan A. Dahlquist · Carmen Galindo · Cesar Casquet · Julio Saavedra

Received: 2 July 2008 / Accepted: 19 April 2009

Abstract The La Costa pluton in the Sierra de Velasco (NW Argentina) consists of S-type granitoids that can be grouped into three igneous facies: the alkali-rich Santa Cruz facies (SCF, SiO_2 ~67 wt%) distinguished by the presence of andalusite and Na- and Li-rich cordierite (Na_2O = 1.55–1.77 wt% and Li_2O = 0.14–0.66 wt%), the Anillaco facies (SiO_2 ~74 wt%) with a significant proportion of Mn-rich garnet, and the Anjullón facies (SiO_2 ~75 wt%) with abundant albitic plagioclase. The petrography, mineral chemistry and whole-rock geochemistry of the SCF are compatible with magmatic crystallization of Na- and Li-rich cordierite, andalusite and muscovite from the peraluminous magma under moderate *P–T* conditions (~1.9 kbar and ca. 735°C). The high Li content of cordierite in the SCF is unusual for granitic rocks of intermediate composition.

P. H. Alasino (✉)
UNLaR, CRILAR-CONICET,
Entre Ríos y Mendoza, 5301 Anillaco, Argentina
e-mail: palasino@crilar-conicet.com.ar

J. A. Dahlquist
UNLaR, CICTERRA-CONICET-UNC,
Av. Vélez Sarsfield 1611, Pab. Geol.,
X5016CGA Córdoba, Argentina

C. Galindo · C. Casquet
Dpto. Petrología y Geoquímica,
UCM, Universidad Complutense, IGE (CSIC),
28040 Madrid, Spain

J. Saavedra
CSIC, Instituto de Agrobiología y Recursos Naturales,
37071 Salamanca, Spain

Keywords Andalusite · Na- and Li-rich cordierite · S-type granite · La Costa pluton · Sierras Pampeanas

Introduction

Andalusite and cordierite are important and common rock-forming minerals in metapelitic rocks and may also be abundant in felsic peraluminous igneous rocks such as granites, pegmatites, aplites and rhyolites. A fundamental question concerning the presence of andalusite and cordierite in peraluminous rocks is how they formed, i.e. whether they crystallized from the magma or were trapped as xenocrysts (e.g. Flood and Shaw 1975; Clarke et al. 1976, 2005; Bellido and Barrera 1979; Phillips et al. 1981; Allen and Barr 1983; Weber et al. 1985; Didier and Dupraz 1986; Georget and Fourcade 1988; Clarke 1995; Erdmann et al. 2004; Gottesmann and Förster 2004; Dahlquist et al. 2005). We have focused here on the petrography, mineral chemistry, and the bulk major and trace element composition of the Santa Cruz igneous facies of the La Costa peraluminous granite pluton in the province of La Rioja, NW Argentina, which contains Na- and Li-rich cordierite, andalusite and muscovite. The occurrence of Na-rich cordierite has been reported in some felsic to highly felsic granitoids (SiO_2 >71 wt%, e.g. Erdmann et al. 2004; Villaseca and Barbero 1994). However, the presence of Na-rich cordierite in granitic rocks of relatively low silica contents such as the Santa Cruz igneous facies (SiO_2 = 65.4–68.6 wt%) has not been found in the literature so far. We provide evidence that supports a magmatic origin for these minerals and evaluate the substitution mechanism that led to this distinctive cordierite composition. Crystallization pressure and temperature values for the La Costa pluton have also been estimated to constrain the physical conditions of

Published online: 16 May 2009

formation of igneous muscovite, andalusite, and Na- and Li-rich cordierite.

Geological setting and geochemistry of the La Costa pluton

The La Costa pluton is a major igneous body in the northeastern part of the Sierra de Velasco (Alasino et al. 2006). Andalusite and Na- and Li-rich cordierite coexist in the Santa Cruz igneous facies, an alkali-rich peraluminous granite with relatively low silica content (SiO_2 = 65.4–68.6 wt%), which constitutes the northern part of the pluton (Fig. 1). Alasino et al. (2005) provided a first detailed account of the field relationships, petrography and whole-rock chemistry of the Santa Cruz igneous facies. Subsequently, Alasino et al. (2006) recognized two additional granitic igneous facies to the south, the Anjullón and the Anillaco, and proposed that the three igneous facies define a single body, named the La Costa pluton.

The La Costa pluton rocks are two-mica alkali-rich leucocratic monzogranites and alkali feldspar granites, with muscovite always prevalent over biotite, with equigranular texture and medium grain-size (4–5 mm). They have no visible foliation and sharp contacts against Carboniferous porphyritic monzogranites (with Pl–Kfs–Qtz–Bt and Ms–Ap–Mon–Zrn as accessories, abbreviations after Kretz 1983) of the Asha pluton and granitic mylonitic rocks (Pl–Kfs–Qtz–Bt–Ms–Grt) of the Tinogasta-Pituil-Antinaco (TIPA) shear zone (López and Toselli 1993; Höckenreiner et al. 2003; Alasino 2007) (Fig. 1b). Each igneous facies of the La Costa pluton is lithologically homogeneous. The modal data are summarized in Table 1. The Santa Cruz igneous facies is distinguished by the presence of andalusite and Na-and Li-rich cordierite; it has a monzogranitic composition. The Anillaco igneous facies (SiO_2 ~74 wt%, monzogranite in composition) is distinguished by containing Mn-rich garnet (spessartine between 42 and 48% of the total molecular composition). The Anjullón igneous facies (SiO_2 ~75 wt%), an alkali-feldspar granite, is characterized by abundant tourmaline and albite ($An_{1.1}$) (Alasino et al. 2006; Alasino 2007). The parental magmas of La Costa pluton were inferred to have resulted from partial melting of metapelitic protoliths within the TIPA shear zone (Alasino 2007).

The La Costa pluton rocks show relatively high Al_2O_3 (13.82–18.01 wt%), Na_2O (3.45–3.93 wt%), K_2O (3.97–5.99 wt%), P_2O_5 (0.27–0.76 wt%), intermediate to low total iron (1.02–2.28 wt% Fe_2O_3) and low MgO (0.03–0.91 wt%), TiO_2 (0.02–0.27 wt%), MnO (0.05–0.14 wt%) and CaO (0.40–1.17 wt%) (Alasino et al. 2006; Alasino 2007). They are peraluminous, with ASI [molecular Al_2O_3/((CaO–P_2O_5) + Na_2O + K_2O)] ≥ 1.1, and are distinctively enriched in some trace elements such as Cs (22–162 ppm), Rb (359–778 ppm), Be (4–22 ppm), Bi (2–216 ppm), Li (137–526 ppm), U (4–27 ppm), Sn (5–43 ppm), W (5–35 ppm), Zn (33–105 ppm), Nb (18–46 ppm), Ga (18–25 ppm) and B (tourmaline in the Anjullón igneous facies can amount to 5 modal %) (Alasino et al. 2006; Alasino 2007). Moreover, they are depleted in Cr, Ni, Co and REE (particularly the Anjullón and the Anillaco igneous facies, ΣREE = 10–18 and 20–25 ppm, respectively) (Alasino et al. 2006; Alasino 2007). The Santa Cruz facies shows the highest contents of TiO_2, Al_2O_3, FeO, MgO, CaO, K_2O and some trace elements such as Be, Sr, Ba, Zr and REE. Whole-rock chemical analyses of the Santa Cruz igneous facies are summarized in Table 2.

Analytical methods

Petrographic investigations were conducted on 29 samples. Electron microprobe analyses were determined on two selected samples using a JEOL Superprobe JXA-8900-M equipped with five crystal spectrometers at the Luis Brú Electron Microscopy Center, Complutense University, Madrid, Spain. Operating conditions were: acceleration voltage 15 kV, probe current 20 nA, and

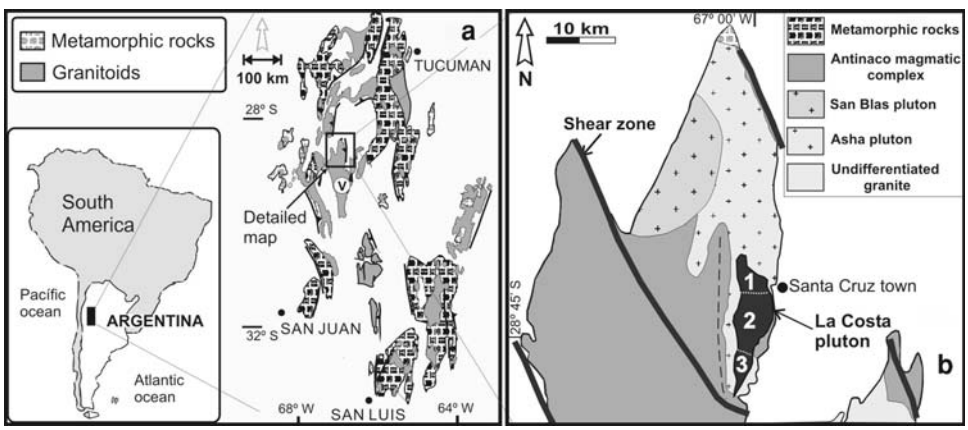

Fig. 1 **a** Geological sketch map of the Sierras Pampeanas showing the location of the Sierra de Velasco (V). **b** Studied area showing location of the La Costa pluton and its igneous facies. *1* Santa Cruz igneous facies, *2* Anjullón igneous facies and *3* Anillaco igneous facies (Alasino et al. 2006; Alasino 2007). *Dotted line* in the Antinaco magmatic complex corresponds to secondary shear zone

Table 1 Representative modal compositions of the La Costa pluton

Igneous facies	Santa Cruz	Anillaco	Anjullón
Number of samples	4	3	4
Total points	991	903	815
Modal %			
Qtz	27.6 ± 1.4	36.1 ± 0.8	43.3 ± 5.5
Kfs	27.1 ± 1.0	18.8 ± 0.9	12.6 ± 2.6
Pl	31.5 ± 0.6	31.7 ± 2.6	30.9 ± 1.9
Bt	3.5 ± 1.5	2.6 ± 0.6	1.9 ± 1.4
Ms	6.9 ± 1.4	7.6 ± 1.1	7.2 ± 1.1
Crd	1.5 ± 0.5	–	–
Grt	–	2.4 ± 0.9	–
And	0.3 ± 0.3	–	–
Tur	0.5 ± 0.1	0.3 ± 0.1	3.3 ± 1.7
Ap	0.4 ± 0.1	0.2 ± 0.0	0.5 ± 0.1
Zrn + Mon	0.4 ± 0.1	0.1 ± 0.0	0.1 ± 0.0
Opq	0.3 ± 0.0	0.2 ± 0.1	0.2 ± 0.1

Mineral abbreviations from Kretz (1983)

beam diameter 1–2 μm. Absolute abundances for each element were determined by comparison with known standards (Jarosewich et al. 1980; McGuire et al. 1992), using an on-line ZAF program. Trace elements were determined in Al-rich minerals and micas for two samples using LA–ICP–MS analyses at Granada University, Spain. The LA–ICP–MS analyses were carried out with a Nd-YAG 213 μm Mercantek laser and a torch-shielded quadrupolar Agilent 7500 ICP-MS spectrometer. The laser beam was set a diameter of 60 μm, with a repetition rate of 10 Hz and output energy of 1 mJ per pulse. The ablation time was 60 s and the spots were pre-abraded for 45 s with laser output energy of 0.3 mJ per pulse; ablation was in a He atmosphere. Every analytical session was started and ended with NIST-610, which was also measured every 6–8 spots. To improve detection limits, blanks (with the laser energy set to zero) were recorded before each spot and subtracted from the analytical signal. Data were reduced using home-made software (freely available from F: Bea) written in STATA programing language (Statacorp 2005). This software permits outliers to be identified and discarded, blank subtraction, drift correction, correction for an external standard and conversion to concentration units on an external standard. The precision, calculated as the coefficient of variation (100 × SD/average) on ten replicates of NIST-6 measured in every session, was about ±3%.

Three samples were chosen for whole-rock chemical analysis, including some major and trace elements (ICP-OES at Alex Stewart Assayers, Argentina SA). In addition, two whole-rock analyses from Alasino et al. (2005) were included in this study (ICP and ICP-MS, following the procedure 4-Lithoresearch code at Activation Laboratories, Ontario, Canada).

Table 2 Representative whole rock chemical analyses for the Santa Cruz igneous facies (La Costa pluton)

Sample no.	SVC-1a[a]	SVC-4a[a]	SVC-104[b]	SVC-105[b]	SVC-106[b]
wt%					
SiO_2	65.36	68.62			
TiO_2	0.27	0.21			
Al_2O_3	18.01	16.82	17.38	17.19	15.82
Fe_2O_3	2.28	1.47		2.27	2.97
MnO	0.08	0.05	0.11	0.08	0.06
MgO	0.91	0.52	0.86	0.75	0.48
CaO	1.17	0.93	1.35	1.21	0.90
Na_2O	3.45	3.52	3.49	3.57	3.22
K_2O	5.67	5.99	5.51	5.70	6.00
P_2O_5	0.52	0.43	0.54	0.48	0.41
LOI	1.24	0.98			
Total	98.96	99.54			
ppm					
Li			180	152	137
Be	22	14			
Cs	49.4	47.4			
Rb	362	359			
Sr	116	104	123	117	100
Ba	517	436	472	466	428
Zr	116	95.5	101	99	83
La	28.4	21.1	28	27	22
Ce	61.9	44.9			
Pr	6.85	5.07			
Nd	26.4	19.8			
Sm	6.32	4.69			
Eu	1.25	1.10			
Gd	5.53	4.24			
Tb	1.05	0.79			
Dy	5.49	4.28			
Ho	0.95	0.76			
Er	2.55	1.99			
Tm	0.34	0.28			
Yb	1.96	1.57			
Lu	0.29	0.23			
ΣREE_{total}	149	111			
ASI	1.42	1.30	1.35	1.31	1.27

Total iron as Fe_2O_3. Al_2O_3, Fe_2O_3, MnO, MgO, CaO, Na_2O and P_2O_5 in SVC-104, 105 and 106 were measured as cations and converted into oxides

[a] Data from Alasino et al. (2005) obtained by ICP and ICP-MS at ACTLABS (Canada)

[b] Data obtained by ICP-OES at Alex Stewart Assayers Argentina SA

Mineral texture and chemistry of the Santa Cruz igneous facies

We focus here on the texture and mineral chemistry of andalusite and Na- and Li-rich cordierite of the Santa Cruz igneous facies as well as on biotite and muscovite that probably crystallized in chemical equilibrium with them, and are thus relevant to our interpretation of the crystallization history.

Andalusite

Andalusite is an accessory mineral in the Santa Cruz igneous facies (<0.6 modal %). It is usually found as small (≤1.2 mm) irregular relic grains armored by muscovite either polycrystalline or large single plates (Figs. 2a–c, 3a). Former andalusite crystals were euhedral to subhedral prismatic, with still recognizable cleavage and without chiastolite (carbonaceous material) or mineral inclusions. They show pink to colorless pleochroism. According to the textural classification by Clarke et al. (2005) of andalusite in felsic peraluminous igneous rocks, the Santa Cruz andalusite corresponds to the "*single -type*" (Figs. 2, 3), i.e. single andalusite grains with or without muscovite pseudomorphs (either mono or polycrystalline).

Electron microprobe analyses of andalusite are shown in Table 3. Some spot locations are shown in Fig. 3a for illustrative purposes. The compositions are very similar to those reported for other andalusites crystallized from a magma (D'Amico et al. 1981; Gordillo et al. 1985; Kawakami 2002; Clarke et al. 2005), i.e. Al_2O_3 between 62.90 and 64.26 wt%, and small amounts of Fe_2O_3 (0.42–0.51wt%). An anomalously high K_2O value of 0.43 wt% probably resulted from interference with muscovite.

The LA–ICP–MS results are reported in Table 4. Trace element contents are generally low, with Li (except one of 113 ppm), Co, Ni, Cu lower than 1 ppm and Sc, Cr, Zn ranging from 1 to 20 ppm. The REE contents are below detection limits except for one sample that shows measurable light REE (La, Ce, Pr and Nd). P, Ga, and V contents are high with range: 71–204, 126–168 and 120–161 ppm, respectively (Table 4; Fig. 4).

Na- and Li-rich cordierite

Cordierite constitutes 1–2% of the mode. It is often found as medium-grained (≤2.5 mm) euhedral to subhedral crystals with a few random inclusions of zircon, apatite and opaque minerals (mainly Fe–Ti oxides). Irregular single grains of cordierite are commonly found armored by polycrystalline muscovite, suggesting subsolidus replacement by the latter mineral (Fig. 3b). In some cases, irregular single grains of cordierite are surrounded by muscovite and biotite and by chlorite after biotite (Fig. 2d). Cordierite and andalusite show a homogeneous distribution in thin section.

Cordierite electron microprobe analysis results are shown in Table 5. Some spot locations are shown in Fig. 3b. The Al_2O_3 content (31.64–32.84 wt%) is high relative to other Na-rich cordierites ($1.65 \leq Na_2O \leq 1.99$ wt% and $28.2 \leq Al_2O_3 \leq 29.5$ wt%) from pegmatites (Gordillo et al. 1985), but is similar to those from felsic monzogranites (e.g. Villaseca and Barbero 1994; Erdmann et al. 2004). However, the Santa Cruz facies cordierite is remarkably rich in Na_2O (1.55–1.77 wt%), which is unusual for cordierites from granitic rocks of relatively low silica content (i.e. between 65 and 68 wt%). The high MnO content (0.85–1.43 wt%) is also remarkable. Contents of K_2O (0.01–0.04 wt%) and CaO (0.01–0.13 wt%), i.e. elements that enter the hexagonal channels of the structure, are low. The X_{Fe} range (0.39–0.60, mean of 13 analyses = 0.47; Table 5) is similar to the compositional range reported for other Na-rich cordierites (Gordillo et al. 1985).

LA–ICP–MS data for the Santa Cruz facies cordierite are reported in Table 4 and Fig. 4. These cordierites show remarkably high concentrations of Li (654–3,043 ppm),

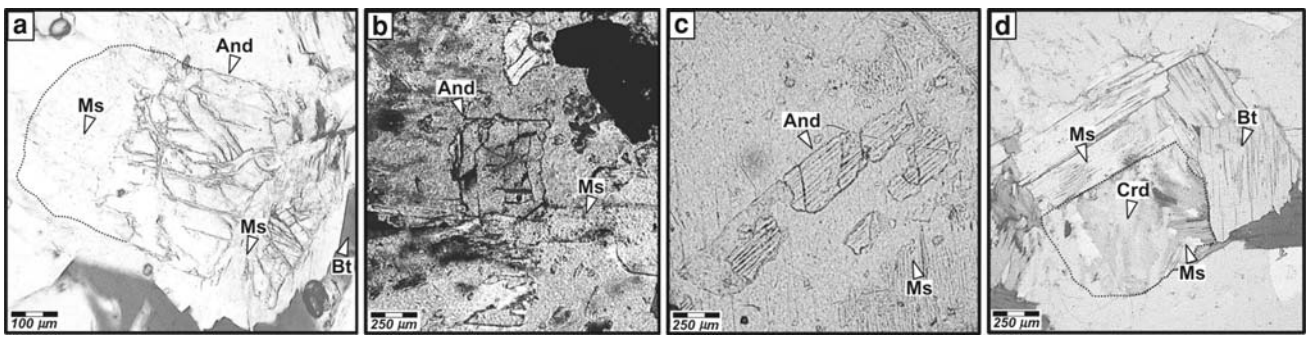

Fig. 2 Photomicrographs showing the textural relationships between andalusite (**a–c**), Na-rich cordierite (**d**) and muscovite from Santa Cruz igneous facies, La Costa pluton: abbreviations mineral after Kretz (1983); **b** and **c** taken from Alasino et al. (2005)

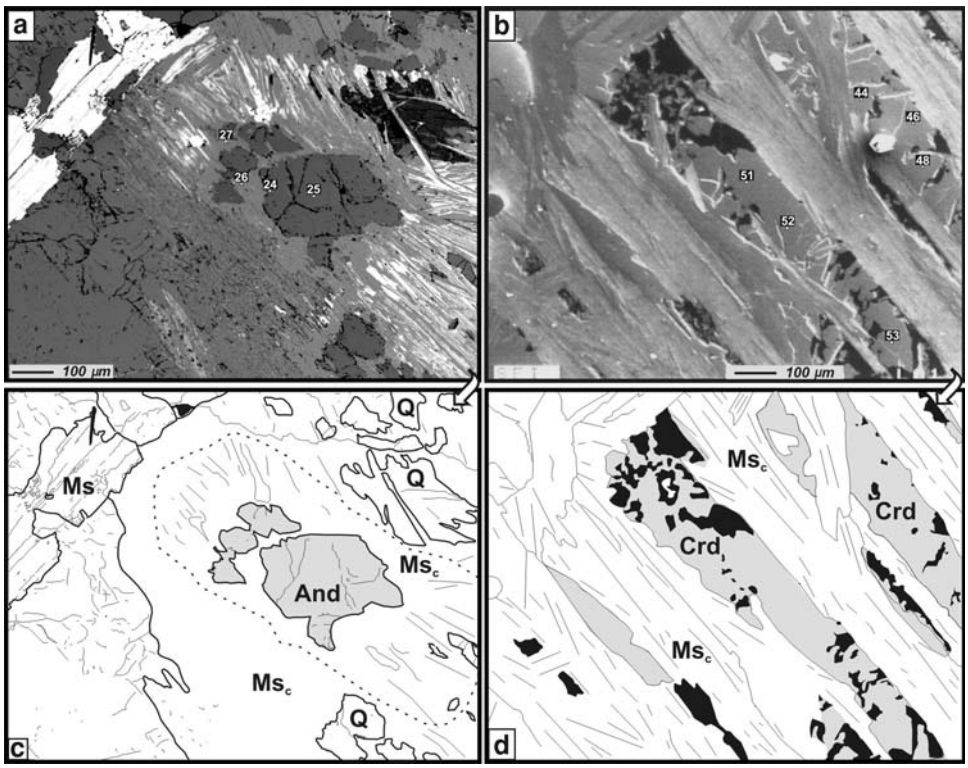

Fig. 3 **a**, **b** BSE images with corresponding sketches (**c**, **d**) showing the location of electron microprobe spots for andalusite, Na-rich cordierite (Tables 3, 5), muscovite from the Santa Cruz igneous facies and textural relationships among them. According to Clarke et al. (2005), textural relationships like those shown here are indicative of subsolidus replacement of muscovite after andalusite and Na- and Li-rich cordierite that resulted in a polycrystalline muscovite pseudomorph. Mineral abbreviations after Kretz (1983)

Rb (7–678 ppm), Zr (9–463 ppm), Cs (162–442 ppm) and Be (82–1,878 ppm). Other trace element contents are: Zn (85–310 ppm), Ba (10–233 ppm), Cu (5–145 ppm), P (20–104 ppm), Ga (19–59 ppm), Sr (3–48 ppm) and Hf (5–42 ppm). Elements such as Sc, V, Cr, Co, Ni, Ta, Pb, Tl, U, Y, Nb and Th are in most cases well below 15 ppm. The total REE content is low (<19.1 ppm); intermediate and heavy REE contents are in most cases below the detection limit.

Substitution mechanisms in Na- and Li-rich cordierite

Several authors (e.g. London 1995; Černý et al. 1997; Evensen and London 2003; Bertoldi et al. 2004) pointed out that Be and Li can be significantly fractionated in cordierite ($D_{\mathrm{Li}}^{\mathrm{Crd/melt}} = 125 \pm 3.7$ and $D_{\mathrm{Be}}^{\mathrm{Crd/melt}} = 29.1 \pm 2.1$; Bea et al. 1994) coincident with coupled Na+ substitution (Gordillo et al. 1985; Schreyer 1985; Bertoldi et al. 2004 and references therein). In fact, the high contents of Li (~0.18 a.p.f.u.) and Na (0.32–0.37 a.p.f.u.) (Table 5) found in cordierite from the Santa Cruz igneous facies correlate well with the low octahedral site occupancy by divalent cations ($\Sigma Mg + Fe^{2+} + Mn = 1.73$ a.p.f.u., average from 13 electron microprobe analyses; Table 5). This evidence suggests that incorporation of Li in cordierite probably resulted from the following coupled substitution (Schreyer 1985) as evidenced in Fig. 5:

$$^{\mathrm{Ch}}\mathrm{Na}^{+} + {}^{\mathrm{VI}}\mathrm{Li}^{+} = {}^{\mathrm{Ch}}[\,] + {}^{\mathrm{VI}}\mathrm{Mg}^{2+}. \quad (1)$$

The introduction of Na^+ in the hexagonal channels of the cordierite crystal structure would involve coupled introduction of Li^+ in the octahedral site, replacing divalent cations. Moreover, the high content of Be in the Santa Cruz facies cordierite (82–1,879 ppm) suggests a coupled substitution (Černý and Povondra 1966) of the type:

$$^{\mathrm{Ch}}\mathrm{Na}^{+} + {}^{\mathrm{IV}}\mathrm{Be}^{2+} = {}^{\mathrm{Ch}}[\,] + {}^{\mathrm{IV}}\mathrm{Al}^{3+}. \quad (2)$$

The high content of Cs in the Santa Cruz facies cordierite (162–442 ppm) is also noticeable. Fractionation of Cs into magmatic cordierite ($D_{\mathrm{Cs}}^{\mathrm{Crd/melt}} = 31.5 \pm 1.6$; Bea et al. 1994) has in fact been invoked by several authors (e.g. London 1995; Černý et al. 1997; Evensen and London 2003; Bertoldi et al. 2004).

Biotite

Biotite is medium-grained (~2.8 × 1.6 mm) euhedral to subhedral, with light- to dark-brown pleochroism. Occasionally small crystals of zircon, monazite and apatite were observed as inclusions.

In terms of Al^{IV} versus $Fe^{2+}/(Fe^{2+} + Mg)$, biotite from the Santa Cruz igneous facies shows high siderophyllite–eastonite contents and intermediate $Fe^{2+}/(Fe^{2+} + Mg)$ ratios between 0.55 and 0.57 (Table 6). Biotite has a

Table 3 Representative composition of the Santa Cruz igneous facies andalusite

Mineral	Andalusite 1		Andalusite 2			
Analysis no.	24	25	59	41	58	60
wt%						
SiO_2	35.75	35.37	36.97	37.28	37.43	37.82
Al_2O_3	64.26	63.21	63.87	63.64	63.65	62.90
TiO_2	0.04	0.05	0.05	bdl	0.03	0.08
Fe_2O_3	0.47	0.51	0.46	0.50	0.46	0.42
MnO	bdl	0.01	bdl	bdl	bdl	bdl
MgO	0.01	0.04	0.06	bdl	0.01	0.03
CaO	bdl	0.01	0.01	bdl	0.02	0.02
Na_2O	bdl	bdl	bdl	bdl	bdl	0.02
K_2O	0.03	0.01	0.03	0.02	0.05	0.43
F	bdl	0.03	bdl	0.03	0.02	0.03
Cl	bdl	bdl	bdl	bdl	bdl	0.01
Total	100.56	99.24	101.45	101.47	101.67	101.76
Structural formulae calculated on the basis of 20 O						
Si	3.85	3.86	3.94	3.97	3.98	4.03
Al	8.15	8.13	8.02	7.99	7.97	7.89
Ti	0.00	0.00	0.00	0.00	0.00	0.01
Fe^{3+}	0.04	0.04	0.04	0.04	0.04	0.03
Mn	0.00	0.00	0.00	0.00	0.00	0.00
Mg	0.00	0.01	0.01	0.00	0.00	0.01
Ca	0.00	0.00	0.00	0.00	0.00	0.00
Na	0.00	0.00	0.00	0.00	0.00	0.01
K	0.03	0.01	0.02	0.05	0.03	0.43

Total iron measured as FeO and expressed as Fe_2O_3. Andalusite 1 and 2 correspond to different analyzed mineral grains

bdl below detection limit

Table 4 Representative LA–ICP–MS analyses of the Santa Cruz igneous facies Al-rich minerals

Mineral	Andalusite			Cordierite 1		Cordierite 2	
Analysis no.	23	24	25	7	8	31	32
ppm							
Li	0.95	1.01	113	3,042	2,978	1,236	654
Be	bdl	0.04	0.64	205	1,878	82.0	86.5
Cs	bdl	bdl	bdl	161	229	442	281
P	132	204	71.2	18.9	103	94.5	49.1
Sc	2.93	2.39	1.38	2.34	2.23	3.21	1.75
V	160	160	119	0.85	0.90	4.38	1.93
Cr	7.57	16.9	18.3	5.66	bdl	3.76	bdl
Co	0.36	0.30	0.21	9.88	4.64	15.0	8.40
Ni	0.44	0.67	0.46	2.88	4.23	11.8	4.28
Cu	0.13	0.07	0.13	0.62	4.96	144	20.2
Zn	8.95	9.79	5.28	171	84.7	310	238
Ga	167	163	125	51.9	58.9	16.8	43.8
Rb	0.07	0.02	bdl	7.44	146	413	678
Sr	bdl	bdl	bdl	3.41	8.75	48.4	10.7
Y	bdl	bdl	bdl	0.45	0.72	5.80	1.06
Zr	bdl	0.03	0.14	13.0	8.67	462	64.3
Nb	bdl	0.02	bdl	0.13	0.11	2.36	0.66
Ba	bdl	0.04	0.02	10.0	134	163	232
Hf	bdl	bdl	bdl	0.02	bdl	42.0	5.15
Ta	bdl	bdl	bdl	bdl	bdl	1.76	0.24
Tl	bdl	bdl	bdl	0.11	1.25	2.51	4.69
Pb	bdl	bdl	bdl	1.22	4.10	16.5	4.77
Th	bdl	bdl	bdl	0.17	0.12	0.79	0.07
U	bdl	bdl	0.05	0.23	0.60	6.46	1.20
REE (ppm)							
La	bdl	bdl	0.17	0.08	bdl	3.83	0.84
Ce	bdl	bdl	0.22	0.10	1.07	5.91	1.42
Pr	bdl	bdl	0.04	0.12	0.13	0.81	0.17
Nd	bdl	bdl	0.16	0.07	bdl	3.60	0.74
Sm	bdl	bdl	bdl	bdl	0.09	0.96	0.07
Eu	bdl	bdl	bdl	bdl	0.05	0.28	0.10
Gd	bdl	bdl	bdl	bdl	bdl	0.96	0.07
Tb	bdl	bdl	bdl	bdl	bdl	0.16	bdl
Dy	bdl	bdl	bdl	bdl	bdl	1.01	bdl
Ho	bdl	bdl	bdl	bdl	bdl	0.22	bdl
Er	bdl	bdl	bdl	bdl	bdl	0.60	bdl
Tm	bdl	bdl	bdl	bdl	bdl	0.09	bdl
Yb	bdl	bdl	bdl	0.27	bdl	0.55	bdl
Lu	bdl	bdl	bdl	0.02	bdl	0.09	bdl

Cordierite 1 and 2 correspond to different analyzed mineral grains

bdl below detection limit

consistently high Al^{IV} content (2.56–2.66 a.p.f.u.; Table 6). The LA–ICP–MS analyses of biotite reveal high concentrations of Li (609–1,032 ppm), Cs (44–877 ppm), Zn (260–673 ppm), V (49–407 ppm) and Nb (96–313 ppm), with lower concentrations of Cr (≤136 ppm), Ga (≤64 ppm), Ta (≤58 ppm), Sc (≤33 ppm), Co (≤31 ppm), Ni (≤26 ppm), Tl (≤11 ppm), Be (≤8 ppm), Pb (≤4 ppm) and low concentrations of Cu, U, Th, Hf (≤2 ppm; Table 7; Fig. 4). The REE total content is low (<8.7 ppm; Table 7).

Muscovite

Care was taken to distinguish between primary and secondary muscovite. Primary muscovite is widely held to be an indicator of peraluminous magmas (Speer 1984). Petrographic evidence and chemical data suggest that both types of muscovite are present in the Santa Cruz igneous facies.

Chemical analyses of texturally primary muscovite (see Table 6), i.e. medium-grained ~3.2 × 1.9 mm, euhedral crystals, plot in the expected compositional field on a Mg–Ti–Na diagram (Fig. 6a) according to the criteria of Miller et al. (1981). Moreover, primary muscovite in the Santa

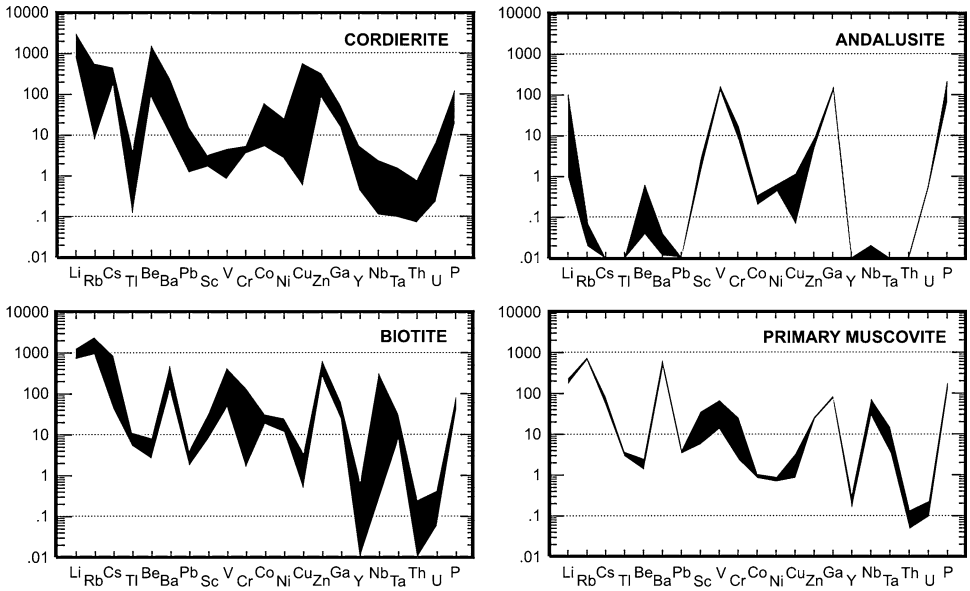

Fig. 4 Absolute abundance plots of trace element contents (ppm) other than REE in cordierite, andalusite, biotite and primary muscovite from the Santa Cruz igneous facies, La Costa pluton

Cruz facies is similar in composition to that coexisting with aluminous minerals (Fig. 6a). The LA–ICP–MS analyses of primary muscovite show relatively high contents of Li (183–221 ppm) and P (103–137 ppm), intermediate contents of Ga (79–86 ppm), Cs (55–88 ppm), Nb (29–77 ppm), V (17–69 ppm) and Zn (24–26 ppm) (Table 8). A few elements such as the transition metals (Sc, Cu, Zr and Ta), Be, Tl and Pb show contents ranging from 1 to 15 ppm. The remaining elements reported in Table 8 (i.e. Ni, Y, Hf, Th and U) are below 1 ppm (see Fig. 4). Total REE content is low (<5.82 ppm; Table 8).

Secondary muscovite is of two types: (1) medium to fine-grained ($\sim 1.1 \times 0.6$ mm) anhedral (Ms_b), grown from biotite or K-feldspar and, (2) polycrystalline (Ms_c), as pseudomorphs and overgrowths after andalusite and/or Na- and Li-rich cordierite (Figs. 2, 3). Electron microprobe analyses of $Ms_{b\text{-}c}$ are shown in Table 6. Secondary muscovite plots in the secondary-mica field of the Mg–Ti–Na diagram (Fig. 6a). Trace element contents in secondary muscovite Ms_c embrace those of primary muscovite (Table 8; Fig. 6b). Relative to primary muscovite, secondary muscovite after cordierite shows lower contents of P, Sc, V, Cr, Y, Nb, Ta, Th and U (Fig. 6b), whereas secondary muscovite after andalusite shows higher contents of those elements than primary muscovite (Fig. 6b). REE content in secondary muscovite is below detection limit (Table 8).

Physical conditions of crystallization of the Santa Cruz igneous facies

Physical conditions of crystallization of the La Costa pluton were determined for the Anillaco igneous facies, which contains Mn-rich garnet (Sps $\sim$46 mol %, see previous section). This granite is similar to other Mn-rich garnet granites (e.g. Dahlquist et al. 2007 and references therein). Anderson (1996) provided relevant recommendations for the use of mineral thermometers and barometers in igneous rocks and concluded that the Ganguly and Saxena (1984) geothermometer, using the Fe^{2+} + Mg partition between garnet and biotite, is the most robust to account for the effects of high Mn, when CaO < 10%. For this reason the Ganguly and Saxena (1984) Fe^{2+}–Mg^{2+} garnet–biotite exchange geothermometer and the R2 and R4 geobarometers of Hoisch (1990) were combined to obtain *P–T* values that can extrapolated to the Santa Cruz igneous facies, particularly pressure. Both gauges require equilibrium crystallization of quartz, garnet, biotite, muscovite and plagioclase. Because both calibrations are *P–T* dependent, an iterative procedure was followed. The resultant values ($T \sim 730$°C, and $P \sim 1.9$ kbar; Table 9) are consistent with crystallization of Mn-rich garnet and biotite under magmatic conditions (e.g. Clemens and Wall 1981; Miller and Stoddard 1981). The zircon saturation temperature (T_{Zr}) calculated from the bulk-rock composition of the Santa Cruz igneous facies using the equation of Miller et al. (2003), is 758°C (Table 9), consistent with that of the Anillaco igneous facies.

Discussion

Evidence for a magmatic origin of andalusite and cordierite

The Santa Cruz facies andalusite and cordierite cannot be interpreted either as part of a restite assemblage resulting from partial melting of a metamorphic protolith (e.g. Flood and Shaw 1975; Zeck and Williams 2002) or as xenocrysts

Table 5 Representative microprobe analyses of the Santa Cruz igneous facies cordierite

Mineral	Cordierite 1		Cordierite 2											Crd[a]
Analysis no.	30	31	44	44′	45	46	47	48	49	50	51	52	54	Av.
wt%														
SiO_2	47.49	47.61	47.01	46.82	47.05	47.50	46.88	48.18	47.58	46.12	47.45	48.04	48.10	47.37
Al_2O_3	32.82	32.67	31.97	31.74	32.49	32.54	32.23	32.18	32.72	31.64	32.92	32.68	32.68	32.41
TiO_2	bdl	bdl	bdl	bdl	bdl	bdl	bdl	bdl	0.04	0.01	0.02	0.03	bdl	0.01
FeO	7.01	6.85	9.88	9.86	9.95	7.27	6.98	6.49	9.63	9.00	7.57	6.69	6.76	8.00
MnO	0.90	1.38	0.89	0.95	0.85	1.29	1.43	1.43	0.97	1.27	0.92	1.21	0.97	1.11
MgO	5.82	5.77	4.08	3.71	4.27	5.42	5.34	5.70	4.41	4.44	5.34	5.60	5.85	5.06
CaO	0.01	0.04	0.08	0.05	0.13	0.07	0.11	0.07	0.07	0.10	0.03	0.06	0.05	0.07
Na_2O	1.58	1.55	1.67	1.64	1.74	1.64	1.76	1.75	1.70	1.77	1.65	1.70	1.63	1.68
K_2O	0.01	bdl	0.04	bdl	0.04	bdl	0.03	0.01	bdl	0.01	bdl	0.01	0.03	0.01
F	bdl	bdl	bdl	0.01	bdl	bdl	bdl	bdl	bdl	0.01	bdl	bdl	bdl	bdl
Cl	bdl	bdl	bdl	bdl	bdl	0.01	bdl	bdl	bdl	0.01	bdl	bdl	bdl	bdl
Li_2O[b]	nd	nd	nd	nd	nd	nd	nd	nd	nd	nd	nd	nd	nd	0.43
BeO[b]	nd	nd	nd	nd	nd	nd	nd	nd	nd	nd	nd	nd	nd	0.16
Total	95.64	95.87	95.62	94.78	96.52	95.74	94.76	95.81	97.12	94.38	95.90	96.02	96.07	96.30
Structural formulae calculated on the basis of 18 O														
Si	5.03	5.04	5.05	5.08	5.02	5.04	5.03	5.09	5.03	5.02	5.03	5.07	5.07	5.01
Al^{IV}	3.97	3.96	3.95	3.92	3.98	3.96	3.97	3.91	3.97	3.98	3.97	3.93	3.93	3.95
Be														0.04
Sum-T	9.00	9.00	9.00	9.00	9.00	9.00	9.00	9.00	9.00	9.00	9.00	9.00	9.00	9.000
Al^{VI}	0.13	0.11	0.10	0.13	0.09	0.12	0.11	0.10	0.11	0.08	0.13	0.13	0.12	0.16
Ti	0.00	0.00	0.00	0.00	0.00	0.00	0.00	0.00	0.00	0.00	0.00	0.00	0.00	0.00
Fe^{2+}	0.62	0.61	0.89	0.89	0.89	0.65	0.63	0.57	0.85	0.82	0.67	0.59	0.60	0.62
Mn	0.08	0.12	0.08	0.09	0.08	0.12	0.13	0.13	0.09	0.12	0.08	0.11	0.09	0.08
Mg	0.92	0.91	0.65	0.60	0.68	0.86	0.85	0.90	0.69	0.72	0.84	0.88	0.92	0.92
Li														0.18
Sum-B	1.75	1.75	1.72	1.71	1.74	1.75	1.72	1.70	1.74	1.74	1.72	1.71	1.73	1.96
Ca	0.00	0.00	0.01	0.01	0.02	0.01	0.01	0.01	0.01	0.01	0.00	0.01	0.01	0.00
Na	0.32	0.32	0.35	0.34	0.36	0.34	0.37	0.36	0.35	0.37	0.34	0.35	0.33	0.33
K	0.00	0.000	0.01	0.00	0.01	0.00	0.00	0.00	0.00	0.00	0.00	0.00	0.00	0.00
Sum-A	0.32	0.32	0.37	0.35	0.39	0.35	0.38	0.37	0.36	0.38	0.34	0.36	0.34	0.33
Fe/(Fe + Mg)	0.40	0.40	0.58	0.60	0.57	0.43	0.42	0.39	0.55	0.53	0.44	0.40	0.39	0.47

Total iron measured as FeO. Cordierite 1 and 2 correspond to different analyzed mineral grains

bdl below detection limit; nd not determined

[a] Corresponds to the average of the analysis of cordierite using the data obtained from electron microprobe (this table) and the data obtained from LA–ICP–MS (Table 4)

[b] Data obtained from the average of Li and Be from Table 4 and converted into oxides

added to the magma from metamorphic country rock (e.g. Ugidos and Recio 1993; Stimac et al. 1995; Gottesmann and Förster 2004).

1. *Field evidence* Andalusite and cordierite were only found in the Santa Cruz igneous facies, i.e. they are absent in the other two igneous facies of the La Costa pluton, suggesting that both minerals crystallized from the Santa Cruz facies magma. The La Costa pluton was emplaced within undeformed biotite porphyritic granites of the Asha pluton and granitic mylonites of the Antinaco magmatic complex (Fig. 1b). Moreover, metamorphic rocks are not found in the area and metamorphic xenoliths are absent from all three facies of the La Costa pluton (Fig. 1b). Thus, there is no field evidence for a local metamorphic origin of andalusite and cordierite.

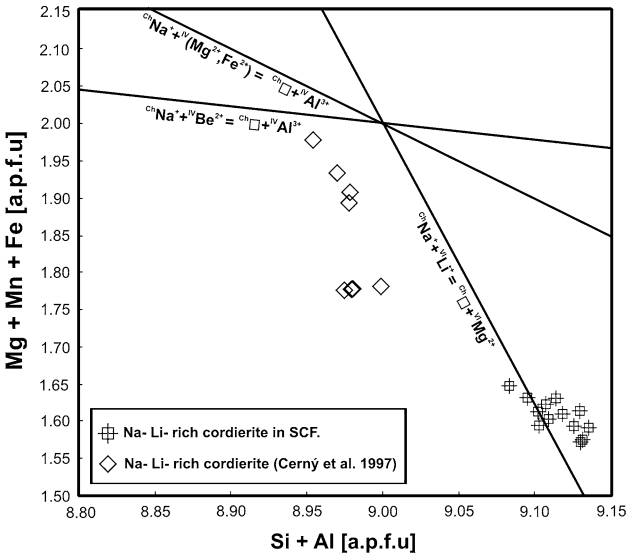

Fig. 5 Octahedral (Mg + Fe + Mn) versus tetrahedral (Si + Al) site occupancy for natural cordierite, ignoring Li and Be in formula calculations (modified from Bertoldi et al. 2004). *SCF* Santa Cruz igneous facies

2. *Textural evidence* The primary texture of both minerals is masked by subsolidus replacement and overgrowth of andalusite and cordierite by muscovite. However, when these minerals are well preserved, they show features typical of igneous crystallization (Erdmann et al. 2004; Clarke et al. 2005), i.e. subhedral to euhedral shapes as opposed to allotriomorphic blastic cordierite, few or no mineral inclusions, absence of chiastolite inclusion in the andalusite, grain-size compatible with the magmatic rock-forming minerals of the Santa Cruz igneous facies, and appearance as homogeneously distributed isolated crystals (surrounded by muscovite). Remarkably, no peritectic texture such as reaction rims on Al-rich minerals (e.g. garnet) or inclusions of high grade metamorphic minerals such as sillimanite were found.
3. *Mineral chemistry* Major element compositions of andalusite provide little information on the mineral origin. However, some information can be gained by checking for chemical equilibrium with other minerals (e.g. biotite, muscovite). The consistently high Al^{IV} content of biotite in all the samples from the Santa Cruz igneous facies is consistent with crystallization in equilibrium with other Al-rich minerals such as andalusite, cordierite and muscovite, a circumstance well-known from other peraluminous rocks with magmatic cordierite or andalusite (e.g. Clarke et al. 2005; Dahlquist et al. 2005). On the other hand, the high Na_2O and MnO contents of the Santa Cruz facies cordierite (Table 5) are remarkable and consistent with a magmatic origin (e.g. Gordillo et al. 1985; Secchi et al. 1991; Villaseca and Barbero 1994; Černý et al. 1997; Rapela et al. 2002; Erdmann et al. 2004; Dahlquist et al. 2005).

Table 6 Representative analyses of the Santa Cruz igneous facies micas

Mineral	Biotite	Muscovite		
Textural type		Ms_a	Ms_b	Ms_c
Analysis no.	Av. ($n = 5$)	Av. ($n = 3$)	33	Av. ($n = 2$)
wt%				
SiO_2	35.09 ± 0.28	45.24 ± 0.31	45.04	45.76 ± 0.10
TiO_2	2.42 ± 0.27	0.26 ± 0.13	bdl	0.04 ± 0.02
Al_2O_3	19.57 ± 0.10	36.09 ± 0.26	36.58	36.28 ± 0.09
FeO	18.96 ± 0.40	1.03 ± 0.10	1.21	0.94 ± 0.21
MnO	0.52 ± 0.02	0.03 ± 0.02	0.02	0.01 ± 0.01
MgO	8.22 ± 0.12	0.76 ± 0.05	0.73	0.74 ± 0.05
CaO	0.02 ± 0.02	0.02 ± 0.02	0.02	0.02 ± 0.00
Na_2O	0.08 ± 0.03	0.54 ± 0.07	0.46	0.44 ± 0.03
K_2O	9.60 ± 0.17	10.77 ± 0.06	10.90	10.98 ± 0.19
F	0.27 ± 0.05	0.06 ± 0.05	0.02	0.03 ± 0.03
Cl	0.04 ± 0.01	0.00	0.02	bdl
Total	94.81 ± 0.68	94.77 ± 0.73	95.00	95.21 ± 0.45
O_F_Cl	0.12 ± 0.02	0.02 ± 0.02	0.01	0.02 ± 0.01
CTotal	94.69 ± 0.67	95.38 ± 0.69	94.99	95.20 ± 0.43
Structural formulae calculated on the basis of 22 O				
Si	5.39 ± 0.05	6.06 ± 0.01	6.03	6.10 ± 0.00
Al^{IV}	2.61 ± 0.05	1.94 ± 0.01	1.97	1.90 ± 0.00
Sum-T	8.00	8.00	8.00	8.00
Al^{VI}	0.93 ± 0.06	3.76 ± 0.03	3.80	3.79 ± 0.03
Ti	0.28 ± 0.03	0.03 ± 0.01	0.00	0.00
Fe^{2+}	2.44 ± 0.05	0.12 ± 0.01	0.14	0.10 ± 0.02
Mn	0.07 ± 0.00	0.00	0.00	0.00
Mg	1.88 ± 0.02	0.15 ± 0.01	0.15	0.15 ± 0.01
Sum-B	5.60	4.06	4.09	4.04
Ca	0.00	0.00	0.00	0.00
Na	0.02 ± 0.01	0.14 ± 0.02	0.12	0.11 ± 0.01
K	1.88 ± 0.02	1.84 ± 0.02	1.86	1.87 ± 0.03
Sum-A	1.90	1.98	1.98	1.98
CF	0.26 ± 0.05	0.05 ± 0.04	0.02	0.03 ± 0.02
CCl	0.02 ± 0.01	0.00	0.01	0.00
Fe/(Fe + Mg)	0.56 ± 0.01	0.43 ± 0.02	0.48	0.41 ± 0.04

Total iron measured as FeO. Muscovite "a" and "b, c" (subscripts) correspond to primary and secondary muscovite, respectively (see text). Abbreviations mineral after Kretz (1983)

bdl below detection limit

Trace elements provide complementary information on the origin of the minerals, particularly for the case of cordierite (e.g. Bea et al. 1994). The high Li content of the Santa Cruz facies cordierite suggests that this mineral crystallized from a Li-enriched magma. Moreover, chemical equilibrium of cordierite with

Table 7 Representative LA–ICP–MS analyses of the Santa Cruz igneous facies biotite

Mineral	Biotite 1			Biotite 2		Biotite 3		Biotite 4	
Analysis no.	1	2	3	19	20	26	27	34	35
ppm									
Li	739	674	609	628	636	903	903	1,032	956
Be	4.12	3.49	3.05	2.74	3.54	4.44	5.03	8.48	6.50
Cs	876	700	639	44.0	55.5	178	93.0	754	304
P	88.3	77.3	71.2	55.2	47.0	42.2	46.2	82.9	64.4
Sc	12.4	9.49	8.16	27.6	32.6	16.6	24.2	8.54	10.8
V	70.1	57.5	48.6	347	407	388	347	63.2	150
Cr	2.38	3.06	1.79	132	136	76.8	99.3	2.84	28.8
Co	22.8	19.5	17.1	20.0	18.7	31.2	30.4	23.3	24.5
Ni	14.8	12.1	11.5	15.4	14.5	24.9	26.4	15.0	14.6
Cu	1.82	1.34	1.65	2.18	3.78	0.62	3.48	0.84	0.50
Zn	409	350	310	312	259	673	650	605	585
Ga	37.8	32.7	29.7	37.0	33.8	64.0	57.5	34.4	26.7
Rb	1,666	1,531	1,355	943	925	2,243	2,135	2,009	2,414
Sr	3.96	4.71	5.61	7.22	5.09	0.65	0.97	0.90	0.75
Y	0.54	0.59	0.71	0.50	0.68	0.03	0.04	0.10	bdl
Zr	17.0	18.7	23.2	16.2	23.6	0.34	2.09	3.67	1.22
Nb	110	96.3	88.0	107	105	261	213	126	312
Ba	174	166	172	157	111	523	361	494	110
Hf	0.12	0.23	0.03	0.46	0.62	0.08	0.12	0.09	0.10
Ta	13.9	17.5	15.8	7.49	7.22	24.4	28.6	30.2	58.1
Tl	10.6	9.77	8.16	5.92	6.32	11.3	10.7	10.0	10.5
Pb	3.98	3.61	3.86	4.10	4.14	3.05	3.35	1.95	1.84
Th	0.21	0.24	0.26	0.20	0.23	bdl	bdl	0.03	bdl
U	0.37	0.35	0.43	0.25	0.41	0.05	0.19	0.04	0.06
REE (ppm)									
La	0.67	1.02	0.12	0.64	0.87	0.14	0.04	0.09	0.04
Ce	0.79	1.10	0.15	1.14	1.35	0.21	0.04	0.10	0.06
Pr	1.02	1.47	0.18	0.11	0.15	0.03	bdl	bdl	bdl
Nd	0.45	0.55	0.05	0.48	0.67	0.04	0.02	0.09	bdl
Sm	0.32	0.50	0.07	0.13	0.10	bdl	bdl	bdl	bdl
Eu	2.19	3.55	0.38	0.04	0.02	bdl	bdl	bdl	bdl
Gd	0.31	0.46	0.02	0.08	0.11	bdl	bdl	0.02	0.02
Tb	0.52	bdl	bdl	bdl	bdl	bdl	bdl	bdl	bdl
Dy	bdl	bdl	bdl	bdl	bdl	bdl	bdl	bdl	0.03
Ho	bdl	bdl	bdl	bdl	bdl	bdl	bdl	bdl	bdl
Er	bdl	bdl	bdl	bdl	bdl	bdl	bdl	bdl	bdl
Tm	bdl	bdl	bdl	bdl	bdl	bdl	bdl	bdl	bdl
Yb	bdl	bdl	bdl	bdl	bdl	bdl	bdl	bdl	bdl
Lu	bdl	bdl	bdl	bdl	bdl	bdl	bdl	bdl	bdl

Biotite 1, 2, 3 and 4 correspond to different analyzed mineral grains

bdl below detection limit

andalusite, biotite and primary muscovite in a magma is also suggested by the fact that the four minerals show high contents of trace elements such as Li, Rb, Cs, Zn, Ga and V.

4. *Whole-rock chemistry* The high ASI values (1.27–1.42; Table 2) of the Santa Cruz igneous facies suggest that the granitic magma was saturated in alumina, making precipitation of single cotectic grains of cordierite and andalusite highly probable (D'Amico et al. 1981; Gordillo et al. 1985; Clarke 1995; Dahlquist et al. 2005; Clarke et al. 2005 and references therein). In addition, Patiño Douce (1992) has shown that the activity coefficient of Al in silicic melts is a function of the alkali content of the melt, whereby alkali-rich

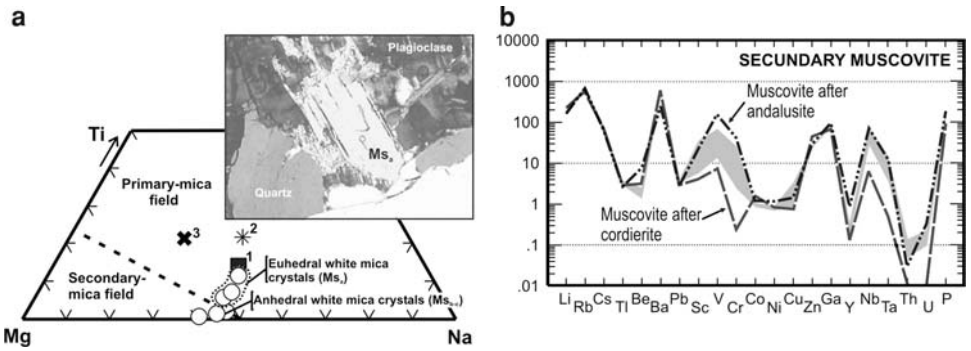

Fig. 6 **a** Mg–Ti–Na diagram to distinguish between secondary and primary muscovite (Miller et al. 1981). The photomicrograph shows a primary muscovite crystal (Ms_a). **b** Absolute abundance plots of trace elements other than REE in secondary muscovite formed from andalusite and cordierite (average from Table 8). The *gray field* corresponds to the primary muscovite from the Santa Cruz igneous facies. References: *1* average muscovite from plutonic rocks with andalusite (Clarke et al. 2005), *2* average muscovite from Tuaní Granite (Dahlquist et al. 2005) and *3* average muscovite from Peñón Rosado Granite (Dahlquist et al. 2007)

melts of similar normative corundum content to alkali-poor melts can crystallize garnet, cordierite, or even aluminosilicates. The La Costa pluton (an alkali-rich melt) is thus a very favorable environment for crystallization of Al-rich minerals.

Crystallization conditions of Al-rich minerals

Primary muscovite and andalusite

Curve SCF in Fig. 7 is the inferred *P–T* path for the Santa Cruz igneous facies. According to this curve, the muscovite in the Santa Cruz igneous facies should be subsolidus if the generally accepted *P–T* locations of the wet granite solidus and the equilibrium curve for the reaction Ms + Qtz = Kfs + Al-silicates + H_2O (e.g. Pattison and Tracy 1991) are correct (curves 1 and Ms; Fig. 7). This however contradicts growing evidence for late magmatic muscovite in many moderate-depth (~1–2 kbar) intrusions (e.g. Dahlquist et al. 2005 and references therein). Moreover, textural and chemical evidence presented here points to a primary origin for some of the muscovites in the Santa Cruz igneous facies. It is well known that addition of P, Li, F and B to peraluminous magmas depresses the granite solidus to lower temperatures at any given pressure (Clarke et al. 2005 and reference therein). The presence of some tourmaline (ca. 0.5 modal %), along with contents of P_2O_5 (ca. 0.50 wt%) and Li (152–180 ppm), and of some F (inferred from the F content of biotite and fluor-apatite) (Tables 2, 6), suggest that the Santa Cruz granitoid solidus was slightly depressed. However, a more important factor for primary muscovite crystallization is the depressing effect on the solidus due to excess Al_2O_3 (~30°C at 2 kbar; Johannes and Holtz 1996) (curve 2; Fig. 7). In fact the Santa Cruz igneous facies has a very high Al_2O_3 content (up to 18 wt%). On the basis of petrographic and geological data, D'Amico et al. (1981) proposed an empirical extension of the muscovite stability field (Ms + Qtz = Kfs + Al-silicates + H_2O/Melt) in water-undersaturated peraluminous granitic melts (curve Ms′; Fig. 7); together with depression of the solidus resulting from coupled Al saturation and fluxing elements; this would permit muscovite crystallization at a pressure of ca. 2 kbar for magmatic temperatures of ca. 700°C (Fig. 7).

According to the andalusite–sillimanite equilibrium curve of Pattison (1992), at temperatures close to the wet granite solidus—at moderate to low pressure—andalusite is the stable form over a relatively large igneous *P–T* field (Fig. 7; curves 1 and P92—field A) (e.g. Cesare et al. 2003; Larson and Sharp 2003). However, the latter field decreases significantly if the andalusite–sillimanite equilibrium curve of Holdaway and Mukhopadhyay (1993) is considered, even compared with the Al_2O_3-saturated granite solidus (Johannes and Holtz 1996) (field B, Fig. 7). Grambling and Williams (1985) showed that small amounts of Fe^{3+} and/or Mn^{3+} in andalusite shift the andalusite–sillimanite boundary significantly upwards. For the case of the Santa Cruz facies andalusite with Fe_2O_3 contents between 0.42 and 0.51 wt% (Table 3), a shift of 13°C has been applied to the HM93 and P92 curves (Fig. 7, HM′ and P′ respectively), values estimated from Kerrick and Speer (1988). However, andalusite can only crystallize to the right of the Ms curve (i.e. the peritectic involving aluminium silicate and muscovite) which implies pressures well below those estimated for the Santa Cruz igneous facies. In consequence the andalusite–sillimanite boundary HM93 for our example seems unrealistic. The andalusite–sillimanite boundary P92 of Pattison (1992), particularly if corrected for the Fe^{3+} content of

Table 8 Representative LA–ICP–MS analyses of the Santa Cruz igneous facies muscovite

Mineral	Primary muscovite				Secondary muscovite				
	Muscovite 1		Muscovite 2						
Analysis no.	4	5	14	15	28, after And	9, after Crd	10, after Crd	29, after Crd	30, after Crd
ppm									
Li	221	182	203	220	169	403	170	176	174
Be	2.44	1.46	2.53	2.11	7.61	5.19	2.52	2.66	2.40
Cs	88.1	55.0	70.8	74.1	77.7	128	38.6	64.5	55.8
P	122	103	114	137	196	91.9	126	93.0	79.2
Sc	36.3	5.88	8.27	7.69	22.2	2.18	2.23	7.26	5.11
V	68.9	16.8	13.8	24.2	167	3.10	2.13	17.5	7.94
Cr	2.85	0.60	25.4	2.23	40.9	0.98	bdl	bdl	bdl
Co	1.08	1.02	0.88	0.96	1.24	4.15	0.70	0.98	0.86
Ni	0.90	0.78	0.70	0.79	1.18	1.88	0.34	0.40	0.82
Cu	0.86	3.37	1.08	2.23	1.47	1.73	1.15	0.10	0.13
Zn	24.3	24.1	24.2	26.3	29.4	98.8	21.0	33.5	30.3
Ga	86.1	78.9	82.0	81.0	98.7	66.7	76.5	66.6	66.7
Rb	708	652	717	717	664	666	512	628	594
Sr	6.58	7.53	7.11	7.10	3.93	6.01	8.66	5.72	6.27
Y	0.35	0.35	0.22	0.16	0.87	0.17	0.41	bdl	0.02
Zr	11.9	12.7	7.69	6.45	6.10	5.30	12.5	0.81	0.51
Nb	77.5	31.6	29.9	29.2	70.2	4.59	1.59	12.8	6.40
Ba	422	442	569	671	241	367	603	688	755
Hf	0.18	0.05	bdl	0.24	0.37	0.02	bdl	0.07	0.01
Ta	15.5	3.66	4.41	4.16	11.2	0.27	0.07	1.23	0.42
Tl	3.54	2.98	3.53	3.75	2.79	4.31	2.68	2.58	2.38
Pb	3.74	4.06	3.35	3.75	2.84	3.54	4.33	2.32	2.14
Th	0.14	0.14	0.08	0.05	0.03	0.06	0.15	bdl	bdl
U	0.21	0.23	0.10	0.11	0.31	0.22	0.21	0.02	bdl
REE (ppm)									
La	0.58	0.07	bdl	0.15	0.22	bdl	bdl	bdl	bdl
Ce	0.68	0.19	bdl	0.30	0.22	bdl	bdl	bdl	bdl
Pr	0.86	0.13	bdl	0.04	bdl	bdl	bdl	bdl	bdl
Nd	0.29	0.05	bdl	0.18	bdl	0.05	0.22	bdl	bdl
Sm	0.38	0.08	0.03	0.05	bdl	bdl	bdl	bdl	bdl
Eu	1.87	0.42	0.03	0.05	bdl	bdl	bdl	bdl	bdl
Gd	0.06	0.07	bdl	0.02	bdl	bdl	bdl	bdl	bdl
Tb	0.01	0.08	bdl	bdl	bdl	bdl	bdl	bdl	bdl
Dy	0.16	0.04	bdl	0.02	bdl	bdl	bdl	bdl	bdl
Ho	0.22	bdl	bdl	bdl	bdl	bdl	bdl	bdl	bdl
Er	0.49	bdl	bdl	bdl	bdl	bdl	bdl	bdl	bdl
Tm	bdl	bdl	bdl	bdl	bdl	bdl	bdl	bdl	bdl
Yb	0.02	bdl	bdl	bdl	bdl	bdl	bdl	bdl	bdl
Lu	bdl	bdl	bdl	bdl	bdl	bdl	bdl	bdl	bdl

Abbreviations mineral after Kretz (1983). Muscovite 1 and 2 correspond to different analyzed mineral grains

bdl below detection limit

andalusite (P′, Fig. 7), better allows for andalusite crystallization prior to primary muscovite formation (field A′; Fig. 7). Moreover, the field for potentially magmatic andalusite is even larger and probably more realistic, if the Richardson et al. (1969) andalusite–sillimanite equilibrium curve is considered (Fig. 7; curve R69).

Table 9 Geothermobarometry for the La Costa pluton

Calibration method	Mineral assemblage / Zr concentration (ppm)	*P*, *T* values	
		T (°C)	*P* (kbar) (±0.1)
Anillaco igneous facies, sample ANI-03			
Ganguly and Saxena (1984)	Grt–Bt	733[a]	
Hoisch (1990) R2 model	Grt–Bt–Pl–Qtz		1.9
Hoisch (1990) R4 model	Grt–Bt–Ms–Pl–Qtz		1.8
Santa Cruz igneous facies			
Zircon saturation temperature (T_{Zr})[b]	99[c]	758	

Composition of the Anillaco facies garnet (analysis number 14–15–16–21–22–23), biotite (45–46–47–48), muscovite (37–38–39–40–49) and plagioclase (29–30–31–33) in the calculations are mean values from Alasino (2007)

[a] See uncertainty discussion in Ganguly and Saxena (1984) and Anderson (1996)

[b] T_{Zr}=12,900/[2.95 + 0.85*M* + ln(476,000/Zr_{melt})], where $D^{Zr,zircon/melt}$ = (476,000/Zr_{melt}) is the ratio of Zr concentration (ppm) in zircon to that in the saturated melt; M is a compositional factor that accounts for dependence of zircon solubility on SiO_2 content and peraluminosity of the melt [(Na + K + 2Ca)/Al × Si), all values as cation fractions] (Watson and Harrison 1983 with rearranging after Miller et al. 2003)

[c] Zirconium concentration in the Santa Cruz igneous facies from the average of Table 2

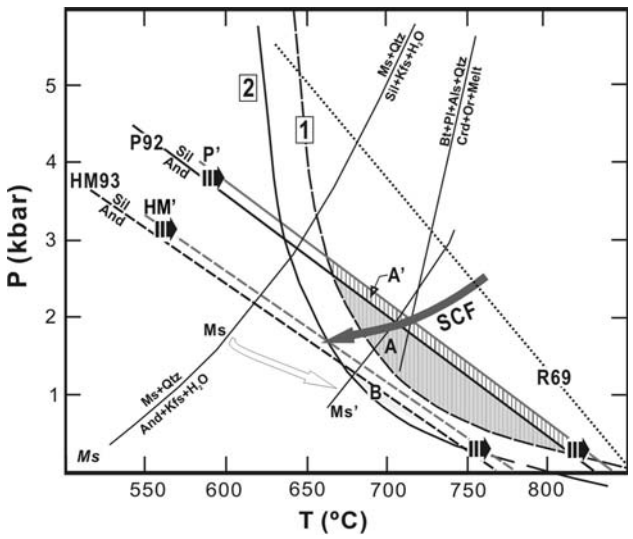

Fig. 7 *P–T* projection illustrating the relationship between the granite solidus, the And-Sill boundary and the Ms + Qtz stability field. *SCF* hypothetical Santa Cruz igneous facies *P–T* path. *A* Field for Al-silicate crystallization prior to primary Ms crystallization, bounded by the wet granite solidus and the And-Sill equilibrium curve P92. *A′* the And + melt field is bounded by the wet granite solidus and the And-Still equilibrium curve *P′*. *B* the And + melt field is bounded by the Al_2O_3-saturated granite solidus and the And-Still equilibrium curve HM′. *1* Wet granite solidus (Johannes and Holtz 1996), *2* Al_2O_3-saturated granite solidus (Johannes and Holtz 1996), *R69* Richardson et al. (1969), *P92* And-Still boundary (Pattison 1992), *HM93* And-Still boundary (Holdaway and Mukhopadhyay 1993). *HM′* and *P′* Shifting of the And-Still boundary (Holdaway and Mukhopadhyay 1993 and Pattison 1992, repectively) due to the Fe^{3+} content of andalusite (see text). *Ms′* empirical equilibrium curve for the reaction: Ms + Qtz = Kfs + Al-silicates + H_2O/Melt (D'Amico et al. 1981). Experimental curves for the reaction Ms + Qtz = Kfs + Al-silicates + H_2O/Melt and Bt + Pl + Al-silicates + Qtz = Crd + Or + Melt are from Pattison and Tracy (1991)

Cordierite

Textural evidence, along with whole-rock and mineral chemical compositions, suggests that Na- and Li-rich cordierite of the Santa Cruz igneous facies crystallized from a peraluminous magma, and that it was at some stage in equilibrium with andalusite (see also Clarke 1995; Erdmann et al. 2004; Clarke et al. 2005; Dahlquist et al. 2005). The chemical composition of the Na- and Li-rich cordierite is consistent with the whole-rock chemistry of the Santa Cruz monzogranite. This granitoid has SiO_2 content (65.3–68.6 wt%; Table 2) remarkably lower than other two other granitic facies of the La Costa pluton (ca. 74 wt%; Alasino et al. 2006). However, the contents of alkalis and other incompatible elements such as Li, Be, Rb and Cs in the Santa Cruz monzogranite are high relative to its silica content (Table 2). It seems that melt composition is the most important single factor controlling mineral/melt partition coefficients. The best constraints on mineral/melt partition coefficients in a low-pressure peraluminous anatectic system are those of Bea et al. (1994), who estimate crystal/melt partition coefficients as the concentration ratios between peraluminous leucosomes (interpreted as pure melts) and mesosome minerals, using a laser probe coupled to an ICP mass spectrometer. These authors demonstrate that cordierite crystallizing in peraluminous magmas strongly fractionates Li, Be, Rb and Cs, and is thus an efficient crystalline reservoir for these elements in magmas strongly enriched in aluminium, at crystallization temperatures of ~750°C, similar that observed for the Santa Cruz igneous facies.

Conclusions

1. The Santa Cruz igneous facies of the La Costa pluton is an S-type granitoid with andalusite, Na- and Li-rich cordierite and primary muscovite. Petrography, mineral chemistry and whole-rock chemistry support magmatic crystallization for all three minerals. Secondary low-*T* muscovite formed under subsolidus conditions, largely after andalusite and Na- and Li-rich cordierite.
2. The Santa Cruz igneous facies crystallized at a moderate depth (ca. 1.9 kbar). At this pressure, crystallization of primary muscovite was favored by both depression of the granite solidus due to Al saturation, and the fluxing effect of B, Li and P in the magma. Moreover, the stability field of muscovite (+quartz) was probably significantly increased relative to the experimental one. Andalusite crystallization from the magma at pressure of ca. 2 kbar implies that the more realistic And-Sill boundary should be that of Pattison (1992) or that of Richardson et al. (1969). Upward shifting by ca. 13°C of the boundary due to Fe^{3+} content in andalusite also contributed to expansion of the andalusite stability field.
3. High Na and Li contents in cordierite are reported for the first time from a relatively low-silica monzogranite. Magma composition was relatively rich in incompatible elements, leading to crystallization of Na-rich cordierite markedly enriched in Li (654–3,043 ppm) and Be (82–1,879 ppm); the micas also show enrichment in some trace elements, such as Rb, Li, Cs, Ba, Nb, Zn, V, P and Sc. Contents of trace elements in andalusite are low except for P, V, Li and Ga.
4. Substitution in the unusual Na- and Li-rich cordierites was of the type: $^{Ch}Na^{+} + {}^{VI}Li^{+} = {}^{Ch}[] + {}^{VI}Mg^{2+}$, leading to almost complete occupancy of the octahedral sites.

Acknowledgments Funds were provided by grants IM-40 2000 (ANPCyT, Argentina), Spanish MEC grant CGL2005-02065/BTE and Universidad Complutense-CAM grant 910495 (2007). We are grateful to C. Villaseca (UCM) for critical review of an earlier draft of this manuscript and to R. Pankhurst (BGS) and P. Searles (CRILAR-CONICET) for revision of the English version of the text. Technical support from CRILAR-CONICET in the preparation of the manuscript is acknowledged. We thank Raúl Lira, Jinhai Yu, Marlina A. Elburg and Wolf-Christian Dullo for insightful and constructive reviews.

References

Alasino P (2007) Geología, petrología y geoquímica de los granitoides Famatinianos ubicados en el sector occidental, y su comparación con el sector central, a los 29° de latitud sur del margen proto-andino de Gondwana, Sierras Pampeanas, Argentina. PhD Thesis, Universidad Nacional de Córdoba (unpblished), Argentina, p 576

Alasino PH, Dahlquist JA, Galindo C, Baldo E, Casquet C (2005) Granitoides peraluminosos con andalucita y cordierita magmáticas en la sierra de Velasco: implicancias para el Orógeno Famatiniano. In: Dahlquist JA, Baldo EG, Alasino PH (eds) Geología de la provincia de La Rioja (Precámbrico—Paleozoico Inferior). Rev Asoc Geol Arg D8:109–122

Alasino PH, Dahquist JA, Galindo C, Casquet C (2006) Plutón La Costa, una expresión de magmatismo tipo–S en el sector noreste de la sierra de Velasco, Sierras Pampeanas, Argentina. Rev Asoc Geol Argent 61:161–170

Allen PL, Barr SM (1983) The Ellison Lake Pluton: a cordierite-bearing monzogranitic intrusive body in southwestern Nova Scotia. Can Mineral 21:583–590

Anderson JL (1996) Status of thermobarometry in granitic batholiths. Trans R Soc Edinb Earth 87:125–138

Bea F, Pereira MD, Stroh A (1994) Mineral/leucosome trace-element partitioning in a peraluminous migmatite (a laser ablation-ICP-MS study). Chem Geol 117:291–312. doi:10.1016/0009-2541(94)90133-3

Bellido F, Barrera J (1979) Nódulos cordieríticos en el granito de La Cabrera (Sistema Central español). Estud Geol 35:279–284

Bertoldi C, Proyer A, Garbe-Schönberg D, Behrens H, Dachs E (2004) Comprehensive chemical analyses of natural cordierites: implications for exchange mechanisms. Lithos 78:389–409. doi:10.1016/j.lithos.2004.07.003

Černý P, Povondra P (1966) Beryllian cordierite from Vezna: (Na, K) + Be → Al. Neues Jahrb Miner Monatsh 44:36–44

Černý P, Chapman R, Schreyer W, Ottolini L, Bottazzi P, McCammon CA (1997) Lithium in sekaninaite from the type locality, Dolni Bory, Czech Republic. Can Mineral 35:167–173

Cesare B, Marchesi C, Hermann J, Gómez-Pugnaire MT (2003) Primary melt inclusions in andalusite from anatectic graphitic metapelites: implications for the Al_2SiO_5 triple point. Geology 31:573–576. doi:10.1130/0091-7613(2003)031<0573:PMIIAF>2.0.CO;2

Clarke DB (1995) Cordierite in felsic igneous rocks: a synthesis. Mineral Mag 59:311–325. doi:10.1180/minmag.1995.059.395.15

Clarke DB, McKenzie CB, Muecke GK, Richardson SW (1976) Magmatic andalusite from the South Mountain Batholith, Nova Scotia. Contrib Mineral Petrol 56:279–287. doi:10.1007/BF00466826

Clarke DB, Dorais M, Barbarin B, Barker D, Cesare B, Clarke G, el Baghdadi M, Erdmann S, Förster H-J, Gaeta M, Gottesmann B, Jamieson RA, Kontak DJ, Koller F, Gomes CL, London D, Morgan Vi GB, Neves LJPF, Pattison DRM, Pereira AJSC, Pichavant M, Rapela C, Renno AD, Richards S, Roberts M, Rottura A, Saavedra J, Sial AN, Toselli AJ, Ugidos JM, Uher P, Villaseca C, Visonà D, Whitney DL, Williamson B, Woodard HH (2005) Occurrence and origin of andalusite in peraluminous felsic igneous rocks. J Petrol 46:441–472. doi:10.1093/petrology/egh083

Clemens JD, Wall VJ (1981) Origin and crystallization of some peraluminous (S-type) granitic magmas. Can Mineral 19:111–131

D'Amico C, Rottura A, Bargossi GM, Nannetti MC (1981) Magmatic genesis of andalusite in peraluminous granites. Examples from Eisgarn Type granites in Moldanubiken. Rend Soc Ital Mineral Petrol 38:15–25

Dahlquist JA, Rapela CW, Baldo E (2005) Petrogenesis of cordierite-bearing S-type granitoids in Sierra de Chepes, Famatinian orogen, Argentina. J S Am Earth Sci 20:231–251. doi:10.1016/j.jsames.2005.05.014

Dahlquist JA, Galindo C, Pankhurst RJ, Rapela CW, Alasino PH, Saavedra J, Fanning CM (2007) Magmatic evolution of the Peñón Rosado granite: petrogenesis of garnet-bearing granitoids. Lithos 95:177–207. doi:10.1016/j.lithos.2006.07.010

Didier J, Dupraz J (1986) Magmatic and metasomatic cordierite in the Velay granitic massif. In: Augusthitis A (ed) The Crust: the significance of granite-gneisses in the lithosphere. Theophrastus, Athens, pp 35–77

Erdmann S, Clarke DB, MacDonald MA (2004) Origin of chemically zoned and unzoned cordierites from the South Montain and Musquodoboit Batholiths, Nova Scotia. Trans R Soc Edinb Earth 95:99–110. doi:10.1017/S0263593304000112

Evensen JM, London D (2003) Experimental partitioning of Be, Cs, and other trace elements between cordierite and felsic melt, and the chemical signature of S-type granite. Contrib Mineral Petrol 144:739–757

Flood RH, Shaw SE (1975) A cordierite-bearing granite suite from the New England batholith, N.S.W., Australia. Contrib Mineral Petrol 52:157–164. doi:10.1007/BF00457291

Ganguly J, Saxena SK (1984) Mixing properties of aluminosilicate garnets: constraints from natural and experimental data, and applications to geothermo-barometry. Am Mineral 69:88–97

Georget Y, Fourcade S (1988) REE partitioning in magmatic cordierite: implications for cordierite-bearing granitoids as exemplified by the Huelgoat intrusion (Brittany, France). Neues Jahrb Miner Abh 158:225–240

Gordillo CE, Schreyer W, Werding G, Abraham K (1985) Lithium in NaBe-cordierites from El Peñón, Sierra de Córdoba, Argentina. Contrib Mineral Petrol 90:93–101. doi:10.1007/BF00373045

Gottesmann B, Förster H-J (2004) Sekaninaite from the Satzung granite (Erzgebirge, Germany): magmatic or xenolithic? Eur J Mineral 16:483–491. doi:10.1127/0935-1221/2004/0016-0483

Grambling JA, Williams ML (1985) The effect of Fe^{3+} and Mn^{3+} on aluminium silicate phase relations in north-central New Mexico, USA. J Petrol 26:324–354

Höckenreiner M, Söllner F, Miller H (2003) Dating the TIPA shear zone: an early Devonian terrane boundary between the Famatinian and Pampean systems (NW Argentina). J S Am Earth Sci 16:45–66. doi:10.1016/S0895-9811(03)00018-X

Hoisch TD (1990) Empirical calibration of six geobarometers for the mineral assemblage quartz + muscovite + biotite + plagioclase + garnet. Contrib Mineral Petrol 104:225–234. doi:10.1007/BF00306445

Holdaway MJ, Mukhopadhyay B (1993) Stability of andalusite and the aluminosilicate phase diagram. Am J Sci 271:97–131

Jarosewich E, Nelen JA, Norberg JA (1980) Reference samples for electron microprobe analysis. Geostand Newsl 4:43–47. doi:10.1111/j.1751-908X.1980.tb00273.x

Johannes W, Holtz F (1996) Petrogenesis and Experimental Petrology of Granitic Rocks. Springer-Verlag, Berlin

Kawakami T (2002) Magmatic andalusite from the migmatite zone of the Aoyama area, Ryoke metamorphic belt, SW Japan, and its importance in constructing the P-T path. J Mineral Petrol Sci 97:241–253. doi:10.2465/jmps.97.241

Kerrick DM, Speer JA (1988) The role of minor element solid solution on the andalusite-sillimanite equilibrium in metapelites and peraluminous granitoids. Am J Sci 288:152–192

Kretz R (1983) Symbols for rock-forming minerals. Am Mineral 68:277–279

Larson T, Sharp Z (2003) Stable isotope constraints on the Al_2SiO_5 "triple-point" rocks from the Proterozoic Priest pluton contact aureole, New Mexico. J Metamorph Geol 21:785–798. doi:10.1046/j.1525-1314.2003.00481.x

London D (1995) Geochemical features of peraluminous granites, pegmatites, and rhyolites as sources of lithophile metal deposits. In: Thompson JFH (ed) Magmas, fluids, and ore deposits. Short Course Handbook, Mineralogical Association of Canada, vol 23, pp 175–202

López JP, Toselli AJ (1993) La faja milonítica TIPA: faldeo oriental del Sistema de Famatina, Argentina. XII Congreso Geológico Argentino 3:39–42

McGuire AV, Francis CA, Diar MD (1992) Mineral standards for electron microprobe analysis of oxygen. Am Mineral 77:1087–1091

Miller CF, Stoddard EF (1981) The role of manganese in the paragenesis of magmatic garnet: an example from the Old Woman Piute Range, California. J Geol 89:233–246

Miller CF, Stoddard EF, Bradfish LJ, Dollase WA (1981) Composition of plutonic muscovite. Genetic implications. Can Mineral 19:25–34

Miller CF, McDowell SM, Mapes RW (2003) Hot and cold granites? Implications of zircon saturation temperatures and preservation of inheritance. Geology 31:529–532. doi:10.1130/0091-7613(2003)031<0529:HACGIO>2.0.CO;2

Patiño Douce AE (1992) Calculated relationships between activity of alumina and phase assemblages of silica-saturated igneous rocks. Petrogenetic implications of magmatic cordierite, garnet and aluminosilicate. J Volcanol Geotherm Res 52:43–63. doi:10.1016/0377-0273(92)90132-W

Pattison DRM (1992) Stability of andalusite and sillimanite and the Al_2SiO_5 triple point: constraints from the Ballachulisch aureole, Scotland. J Geol 100:423–446

Pattison DRM, Tracy RJ (1991) Phase equilibria and thermobarometry of metapelites. In: Kerrick DM (ed) Contact metamorphism. Rev Mineral, vol 26, pp 105–206

Phillips GN, Wall VJ, Clemens JD (1981) Petrology of the Strathbogie batholith: a cordierite-bearing granite. Can Mineral 19:47–63

Rapela CW, Baldo EG, Pankhurst RJ, Saavedra J (2002) Cordieritite and leucogranite formation during emplacement of highly peraluminous magma: the El Pilón Granite Complex (Sierras Pampeanas, Argentina). J Petrol 43:1003–1028. doi:10.1093/petrology/43.6.1003

Richardson SW, Gilbert MC, Bell PM (1969) Experimental determination of kyanite-andalusite and andalusite-sillimanite equilibria: the aluminium silicate triple point. Am J Sci 267:259–272

Schreyer W (1985) Experimental studies on cation substitutions and fluid incorporation in cordierite. Bull Mineral (Paris) 108:273–291

Secchi FA, Brotzu P, Callegari E (1991) The Arburese igneous complex (SW Sardinia, Italy)—an example of dominant igneous fractionation leading to peraluminous cordierite-bearing leucogranites as residual melts. Chem Geol 92:213–243. doi:10.1016/0009-2541(91)90057-X

Speer JA (1984) Micas in igneous rocks. Rev Mineral 13:299–356

Statacorp (2005) STATA statistical software: release 9. Statacorp LP, College Station, TX

Stimac JA, Clark AH, Chen Y, Garcia S (1995) Enclaves and their bearing on the origin of the Cornubian batholith, southwest England. Mineral Mag 59:273–296

Ugidos JM, Recio C (1993) Origin of cordierite-bearing granites by assimilation in the Central Iberian Massif (CIM), Spain. Contrib Mineral Petrol 98:27–43

Villaseca C, Barbero L (1994) Chemical variability of Al-Ti-Fe-Mg minerals in peraluminous granitoids rocks from central Spain. Eur J Mineral 6:691–710

Watson EB, Harrison TM (1983) Zircon saturation revisited: temperature and composition effects in a variety of crustal magma types. Earth Planet Sci Lett 64:295–304. doi:10.1016/0012-821X(83)90211-X

Weber C, Pichavant M, Barbey P (1985) La cordierite dans le domaine anatectique du Velay (Massif Central Français): un marqueur de I'anatexie, du magmatisme et de I'hydrothermalisme. Compt Rend Acad Sci Paris 301:303–308

Zeck HP, Williams IS (2002) Inherited and magmatic zircon from Neogene Hoyazo cordierite dacite, SE Spain–Anatectic source rock provenance and magmatic evolution. J Petrol 43:1089–1104. doi:10.1093/petrology/43.6.1089